Journal Pre-proofs

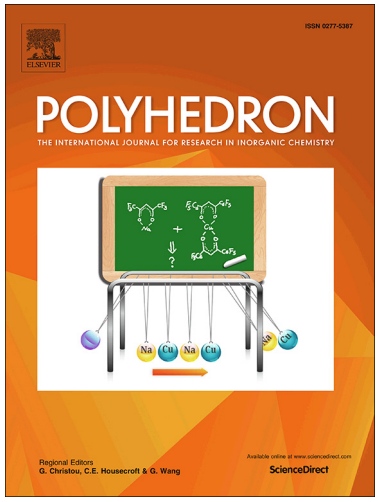

Synthesis and structural characterization of new transition metal complexes of a highly luminescent amino-terpyridine ligand

Biswa Nath Ghosh, Rakesh Puttreddy, Kari Rissanen

PII: S0277-5387(19)30749-1
DOI: https://doi.org/10.1016/j.poly.2019.114304
Reference: POLY 114304

To appear in: *Polyhedron*

Received Date: 16 October 2019
Revised Date: 5 December 2019
Accepted Date: 6 December 2019

Please cite this article as: B. Nath Ghosh, R. Puttreddy, K. Rissanen, Synthesis and structural characterization of new transition metal complexes of a highly luminescent amino-terpyridine ligand, *Polyhedron* (2019), doi: https://doi.org/10.1016/j.poly.2019.114304

Synthesis and structural characterization of new transition metal complexes of a highly luminescent amino-terpyridine ligand

Biswa Nath Ghosh,*[a,b] Rakesh Puttreddy[b] and Kari Rissanen[b]

[a]*Department of Chemistry, National Institute of Technology Silchar, Silchar, Cachar-788010, Assam, Tel: +91-8018123682, E-mail: b.chem06@gmail.com*

[b]*Department of Chemistry, Nano science Center, University of Jyvaskyla, P.O. Box 35, 40014 Jyväskylä, Finland*

Abstract

The synthesis, NMR and UV-Vis spectroscopy measurements and X-ray diffraction analysis of four new metal complexes of the amino terpyridine ligand 4′-[4-(4-aminophenyl)phenyl]-2,2′:6′,2′′-terpyridine **L**, namely [Fe**L**$_2$](ClO$_4$)$_2$ (**1**), [Zn**L**$_2$](ClO$_4$)$_2$ (**2**), [Cd**L**$_2$](ClO$_4$)$_2$ (**3**) and [PtMe$_3$I**L**] (**4**), are reported. The X-ray crystal structures of complexes **1**-**3** are 1:2 metal:ligand structures with tridentate ligands decorated around the octahedral metal centers. In complex **4**, with **L** in a bidentate coordination mode, the Pt(IV) coordinated methyl and iodine groups form a *fac*-arrangement. The ^{1}H NMR spectrum of **4** shows three ^{195}Pt-^{1}H resonances for the methyl groups incorporating the *fac*-arrangement, which confirms the bidentate coordination mode of **L** in solution. The X-ray crystal structure of **L** shows a *transoid* conformation of the pyridine ring nitrogen atoms along the interannular bond in the terpyridine core. Ligand **L** exhibits a bright blue emission in dichloromethane [fluorescence quantum yield (Φ_F) = 68%] and its emission maxima shows significant solvatochromism (461 nm in dichloromethane to 533 nm in N,N-dimethylformamide), while its complexes **2** and **3** are only very weakly emissive and **1** and **4** are found to be non-emissive.

Keywords: Amino terpyridine • Fluorescent • Trimethylplatinum(IV) • Bidentate

Introduction

2,2′:6′,2′′-Terpyridine and its derivatives are well-known in supramolecular chemistry owing to their ability to strongly coordinate transition metal ions [1-4]. In particular, the 4′-functionalized terpyridines and corresponding metal complexes have received considerable attention in areas such as photophysical, electrochemical and catalytic properties [5-9], hydrogelation [10,11], organic light-emitting devices (OLEDs) [12] and mixed-valence chemistry [13,14]. A number of

fluorescent compounds that can act as chemsensors for applications in bio-assays and *in-vivo* imaging purposes are also reported [9,15-23], yet fine tuning of multi-colour fluorescent staining of cell tissues is still a challenging task. Therefore, tuning the fluorophore electronic state for specific cell-staining and fluorophore structural studies remain a hot topic in supramolecular chemistry since any slight structural modifications to the fluorophore brings about unusual fluorescence properties.

Our interest in 4′-functionalized amino terpyridines led us to report the following: i) A highly selective fluorescent sensor based on a 4′-(4-N,N-dimethylaminophenyl)-2,2′:6′,2″-terpyridine-Zn(II) complex for pyrophosphate detection at physiological *p*H values in aqueous media [15]. ii) Ligand and anion effects in the self-assembly processes of divalent transition metal complexes of 4′-(4-N,N-dimethylaminophenyl)-2,2′:6′,2″-terpyridine and 4′-(4-aminophenyl)-2,2′:6′,2″-terpyridine [11]. iii) The ligand 4′-[4-(4-aminophenyl)phenyl]-2,2′:6′,2″-terpyridine (**L**, Scheme 1) as a thermo-irreversible hydrogelator, particularly using Hg(II) salts under acidic conditions [10]. In the current study, we report the synthesis and characterization of four new metal complexes of **L**, [Fe**L**$_2$](ClO$_4$)$_2$ (**1**), [Zn**L**$_2$](ClO$_4$)$_2$ (**2**), [Cd**L**$_2$](ClO$_4$)$_2$ (**3**) and [PtMe$_3$I**L**] (**4**). The X-ray diffraction analysis shows that **L** forms a bidentate complex with the platinum(IV) ion, while tridentate complexes are formed with the divalent metal ions (Fe^{2+}, Zn^{2+} and Cd^{2+}). Further, the crystal structure and photophysical properties of **L** are also reported. The crystal structure of **L** shows a *transoid* conformation of the pyridine ring nitrogen atoms along the interannular bond in the terpyridine domain. A photophysical study shows that **L** is *highly fluorescent in solution* (Φ_F = 0.68 in dichloromethane) with an emission maximum that shows significant solvatochromism. Although **L** is strongly fluorescent, its complexes **2** and **3** are only very weakly emissive, while **1** and **4** are found to be non-emissive.

Experimental section

Materials and methods: All the chemicals and solvents were of analytical reagent grade, purchased commercially and used as received without further purification. The ligand 4′-[4-(4-aminophenyl)phenyl]-2,2′:6′,2′′-terpyridine, **L**, was synthesized following the literature method [10]. The ^{1}H and ^{13}C NMR spectra were recorded on Bruker Avance III HD 300 and DRX 500 spectrometers. The mass spectra were measured on a QSTAR Elite ESI-Q-TOF mass

spectrometer equipped with an API 200 Turbo Ion Spray ESI source from AB Sciex (former MDS Sciex). Elemental analyses were performed with an Elementar Analysensysteme GmbH Vario EL.

Spectroscopic studies: The UV-Visible absorption spectra were recorded on a Cary 100 Varian UV-Vis spectrophotometer, whereas the emission spectra were obtained with a Cary Eclipse Varian Fluorescence spectrophotometer. Fluorescence quantum yields were measured using quinine sulfate as the standard (Φ_F = 0.546 in 0.1 N H_2SO_4). Fluorescence decays in different solvents were measured using a Time-Correlated Single Photon Counting (TCSPC) system consisting of a Hydra Harp 400 controller and a PDL 800-B driver from PicoQuant GmBH. All the spectroscopic measurements were carried out at room temperature and under ambient conditions.

Synthesis of the complex $[FeL_2](ClO_4)_2$ (1): To a degassed acetonitrile solution (5.0 mL) of $Fe(ClO_4)_2.6H_2O$ (19.9 mg, 0.055 mmol), a solution of **L** (44.0 mg, 0.109 mmol) in dichloromethane (20.0 mL) was added and the resulting mixture was stirred at room temperature for 3 h. After this, the solvents were evaporated to dryness, the residue was dissolved in a minimum amount of acetonitrile and excess diethyl ether (30.0 mL) was sequentially added dropwise to give purple coloured precipitates of **1**. Complex **1** was filtered, washed with diethyl ether and dried under vacuum. Yield 90% (52.0 mg). ^{1}H NMR (300 MHz, CD_3CN, 303.15 K) δ/ppm: 9.22 (s, 4H), 8.63 (d, 4H, *J* 7.8 Hz), 8.37 (dt, 4H, *J* 1.8, 8.6 Hz), 8.01 (dt, 4H, *J* 2.0, 8.6 Hz), 7.92 (td, 4H, *J* 1.5, 7.7 Hz), 7.66 (dt, 4H, *J* 1.8, 8.6 Hz), 7.20-7.23 (m, 4H), 7.07-7.12 (m, 4H), 6.84 (dt, 4H, *J* 1.8, 8.5 Hz). MS (ESI-TOF) $[FeL_2]^{2+}$ *m/z* 428.1361 (calcd. 428.1357). UV-Vis, λ_{max} (nm) (dichloromethane): 325, 375, 580. Anal. calcd. for $C_{54}H_{40}Cl_2FeN_8O_8$ (1055.70): C, 61.44; H, 3.82; N, 10.61. Found: C, 61.18; H, 3.92; N, 10.35%.

Synthesis of the complex $[ZnL_2](ClO_4)_2$ (2): To an acetonitrile solution (5.0 mL) of $Zn(ClO_4)_2{\cdot}6H_2O$ (24.6 mg, 0.066 mmol), **L** (53.0 mg 0.132 mmol) dissolved in dichloromethane (15.0 mL) was added and the resulting mixture was stirred at room temperature for 5 h. After this time, the reaction mixture was evaporated to dryness to give a yellow coloured product. The

crude reaction mixture was re-dissolved in a minimum amount of acetonitrile and excess diethyl ether (25.0 mL) was added to precipitate complex **2**. The precipitates were filtered, washed several times with diethyl ether and vacuum dried. Yield 91% (64.0 mg). Slow diffusion of di-isopropyl ether into an acetonitrile solution of **2** gave yellow coloured crystals. ^{1}H NMR (300 MHz, DMSO-d_6, 303.15K) δ/ppm: 9.41 (s, 4H), 9.18 (d, 4H, *J* 8.1 Hz), 8.48 (d, 4H, *J* 8.2 Hz), 8.29 (t, 4H, *J* 7.1 Hz), 7.92-7.97 (m, 8H), 7.63 (d, 4H, *J* 8.6 Hz), 7.48-7.53 (m, 4H), 6.74 (d, 4H, *J* 8.6 Hz). MS (ESI-TOF) $[Zn\mathbf{L}_2]^{2+}$ *m/z* 432.1354 (calcd. 432.1328). UV-Vis, λ_{max} (nm) (dichloromethane): 325, 385. Anal. calcd. for $C_{54}H_{40}Cl_2N_8O_8Zn$ (1065.23): C, 60.89; H, 3.78; N, 10.52. Found: C, 61.17; H, 3.93; N, 10.24%.

Synthesis of $[Cd\mathbf{L}_2](ClO_4)_2$ (3): To an acetonitrile solution (6.0 mL) of $Cd(ClO_4)_2{\cdot}6H_2O$ (21.4 mg, 0.051 mmol), 41.0 mg (0.102 mmol) of **L** dissolved in 15.0 mL dichloromethane was added and the reaction mixture was stirred at room temperature for 7 h. The solvents were removed under reduced pressure and the reaction mixture was re-dissolved in a minimum amount of acetonitrile, then excess of diethyl ether (25.0 mL) was added to precipitate **3** as yellow coloured solids. The precipitates were filtered, washed with diethyl ether and dried under vacuum. Yield 98% (56.0 mg). Single crystals suitable for X-ray diffraction analysis were obtained by slow-diffusion of di-isopropyl ether into an acetonitrile solution of **3**. ^{1}H NMR (300 MHz, DMSO-d_6, 303.15K) δ/ppm: 9.11 (s, 4H), 9.00 (d, 4H, *J* 6.5 Hz), 8.46 (br s, 4H), 8.21-8.27 (m, 8H), 7.86 (d, 4H, *J* 8.4 Hz), 7.54-7.63 (m, 8H), 6.72 (dt, 4H, *J* 1.9, 8.5 Hz). MS (ESI-TOF) $[Cd\mathbf{L}_2]^{2+}$ *m/z* 457.1200 (calcd. 457.1206). UV-Vis, λ_{max} (nm) (dichloromethane): 325, 365. Anal. calcd. for $C_{54}H_{40}CdCl_2N_8O_8$ (1112.26): C, 58.31; H, 3.62; N, 10.07. Found: C, 58.10; H, 3.41; N, 9.82%.

Synthesis of $[PtMe_3I\mathbf{L}]$ (4): A solution of trimethylplatinum iodide (30.0 mg, 0.082 mmol) in chloroform (10.0 mL) was added to **L** (33.0 mg, 0.082 mmol) in chloroform (10.0 mL), and the reaction mixture was stirred at 50 °C for 6 h. The solvents were evaporated under reduced pressure and excess *n*-hexane was added to give a pale-yellow precipitate of **4**. The solids were filtered, washed several times with *n*-hexane and dried under vacuum. Yield 79% (58.0 mg). Also, a 1:1 mixture of trimethylplatinum iodide and **L** in benzene, on standing for a few days, afforded yellow coloured single crystals of the complexes.^{1}H NMR (500 MHz, CD_2Cl_2,

213.15K) δ/ppm: 9.02 (d, 1H, *J* 4.9 Hz), 8.72 (d, 1H, *J* 7.9 Hz), 8.68 (d, 1H, *J* 4.1 Hz), 8.35 (br s, 1H), 8.31 (d, 1H, *J* 7.9 Hz), 8.12 (br s, 1H), 8.08 (t, 1H, *J* 7.7 Hz), 7.79-7.85 (m, 3H), 7.59-7.65 (m, 3H), 7.40-7.44 (m, 3H), 6.71 (d, 2H, *J* 8.11 Hz), 3.99 (s, 2H), 1.49 (s, 3H, $^2J_{Pt-H}$ 73.5 Hz), 0.26 (s, 3H, $^2J_{Pt-H}$ 71.5 Hz), 0.15 (s, 3H, $^2J_{Pt-H}$ 70.4 Hz). MS (ESI-TOF) $[PtMe_3\mathbf{L}]^+$ *m/z* 640.2032 (calcd. 640.2037). UV-Vis, λ_{max} (nm) (dichloromethane): 315, 362. Anal. calcd. for $C_{30}H_{29}IN_4Pt$ (767.57): C, 46.94; H, 3.81; N, 7.30. Found: C, 46.65; H, 3.49; N, 7.05%.

X-ray crystallography

Single crystal X-ray diffraction data for **L**, **2** and **3** were collected using a dual source Rigaku Super Nova Oxford diffractometer equipped with an Atlas CCD detector using mirror-monochromated Cu-Kα radiation (λ = 1.54184 Å). The data collection and reduction were carried out using the program *CrysAlisPro* [24]. The data for **4** was collected using a Bruker-Nonius Kappa CCD diffractometer [25] equipped with an APEX II detector and graphite-monochromatized Mo-*K*α (λ = 0.71073 Å) radiation. *Collect* software was used for data collection [26] and *DENZO-SMN* for its processing [27]. An absorption correction was applied with the multi-scan *SADABS* program [28]. All the structures were solved with direct methods (*SHELXS*) [29] and refined by full-matrix least squares on F^2 using the *OLEX2* software [30], which utilizes the *SHELXL-2015* module [29]. All the hydrogen atoms were calculated to their optimal positions and treated as riding atoms using isotropic displacement parameters either 1.2 or 1.5 larger than the corresponding carrier atoms. Constraints and restraints were used to model disordered structures when necessary.

Crystal data for **L**: CCDC 1901887, $C_{27}H_{20}N_4$, M = 400.47, yellow needle, 0.1567 x 0.053 x 0.0257 mm^3, triclinic, space group *P*-1, a = 9.4598(4) Å, b = 14.2779(6) Å, c = 15.2307(5) Å, α = 96.284(3) °, β = 95.443(3) °, γ = 98.329(4) °, V = 2010.35(14) $Å^3$, Z = 4, Dc = 1.323 g/cm^3, F000 = 840, μ= 0.623 mm^{-1} , T = 123.01(10) K, θ_{max} = 66.75 °, 12197 total reflections, 5681 with Io > 2σ(Io), R_{int} = 0.0301, 7063 data, 561 parameters, 0 restraints, GooF = 1.027, R = 0.0453 and wR = 0.1188 [Io > 2σ(Io)], R = 0.0573 and wR = 0.1286 (all reflections), 0.211 < dΔρ < -0.258 e/$Å^3$.

Crystal data for **2**: CCDC 1901884, $C_{54}H_{40}Cl_2N_8O_8Zn$, M = 1065.21, yellow plate, 0.1949 x0.1015 x0.0558 mm^3, monoclinic, space group $P2_1/c$, a = 22.981(2) Å, b = 8.5117(5) Å, c = 27.206(3) Å, α = 90 °, β = 113.061(13) °, γ = 90 °, V = 4896.3(9) $Å^3$, Z = 4, Dc = 1.445 g/cm^3, F000 = 2192, μ= 0.676 mm^{-1} , T = 173.15 K, θ_{max} = 25.25 °, 32557 total reflections, 4302 with Io > 2σ(Io), R_{int} = 0.0879, 8852 data, 699 parameters, 49 restraints, GooF = 1.053, R = 0.1037 and wR = 0.2888 [Io > 2σ(Io)], R = 0.1916 and wR = 0.3594 (all reflections), 1.186 < dΔρ < -0.509 e/$Å^3$.

Crystal data for **3**: CCDC 1901885, $C_{54}H_{40}CdCl_2N_8O_8$, M = 1112.24, yellow block, 0.2537 x 0.2019 x 0.1658 mm^3, monoclinic, space group $P2_1/c$, a = 23.6891(16) Å, b = 8.4550(4) Å, c = 27.3090(16) Å, α = 90 °, β = 113.003(7) °, γ = 90 °, V = 5034.8(6) $Å^3$, Z = 4, Dc = 1.467 g/cm^3, F000 = 2264, μ= 0.604 mm^{-1} , T = 123.0(1) K, θ_{max} = 25.25 °, 20514 total reflections, 6829 with Io > 2σ(Io), R_{int} = 0.0302, 9103 data, 681 parameters, 31 restraints, GooF = 1.058, R = 0.0817 and wR = 0.2312 [Io > 2σ(Io)], R = 0.1025 and wR = 0.2582 (all reflections), 1.759 < dΔρ < -0.780 e/$Å^3$.

Crystal data for **4**: CCDC 1901886, $C_{36}H_{35}IN_4Pt$, M = 845.67, yellow block, 0.22 x 0.17 x 0.17 mm^3, monoclinic, space group $P2_1/n$, a = 18.8259(18) Å, b = 7.2471(8) Å, c = 23.1917(17) Å, α = 90 °, β = 96.280(5) °, γ = 90 °, V = 3145.1(5) $Å^3$, Z = 4, Dc = 1.786 g/cm^3, F000 = 1640, μ= 5.474 mm^{-1} , T = 123 K, θ_{max} = 25.00 °, 8745 total reflections, 3699 with Io > 2σ(Io), R_{int} = 0.0793, 5277 data, 352 parameters, 32 restraints, GooF = 1.079, R = 0.0795 and wR = 0.1647 [Io > 2σ(Io)], R = 0.1219 and wR = 0.1862 (all reflections), 2.841 < dΔρ < -1.245 e/$Å^3$.

Results and discussion

The ligand **L** was synthesized by the reaction between 4-aminophenylboronic acid pinacol ester and 4′-(4-bromophenyl)-2,2′:6′,2′′terpyridine by following the literature method [10]. Complexes **1-3** were obtained by the reaction of **L** (in dichloromethane) with the metal perchlorate hexahydrate salts (in acetonitrile) in a 2:1 molar ratio, while **4** was prepared by the reaction of **L** with trimethylplatinum(IV) iodide (1:1 molar ratio) in chloroform (Scheme 1). The presence of only one set of signals for the terpyridine core in the room temperature ^1H NMR spectra of complexes **1-3** revealed the tridentate metal-coordination mode of **L**. Unlike **1-3**, the

room temperature ^{1}H NMR spectrum of **4** in CD_2Cl_2 showed severe broadening (see Figure S4 in the supporting information) and thus the ^{1}H NMR spectrum was measured at low temperature (-60 °C) to get a better resolved spectrum. The ^{1}H NMR spectrum of **4** is closely analogous to the spectra of reported Pt^{IV}-terpyridine complexes [23,31,32]. The presence of three platinum-methyl signals with satellites, due to ^{195}Pt-H scalar coupling, revealed the presence of three non-equivalent methyl groups (Me_A, Me_B and Me_C) in complex **4** (Figure 1). The above observation gives an indication that **L** binds the platinum metal centre in a bidentate fashion. The ESI-MS of the symmetric homoleptic complexes **1-3** show the parent molecular ion, $[ML_2]^{2+}$, while **4** displays the molecular ion peak with the loss of iodide, *i.e.* $[PtMe_3L]^{+}$ (see Figures S6-S9 in supporting information).

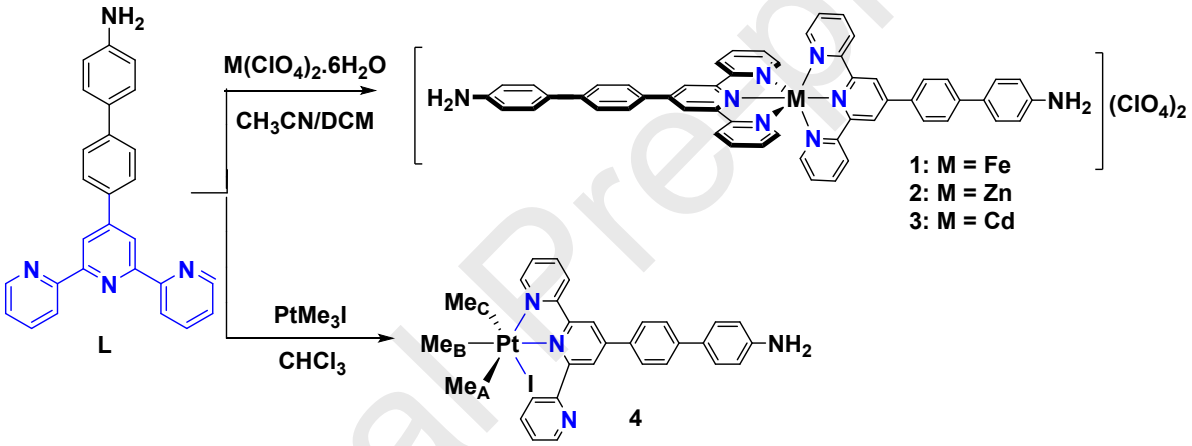

Scheme 1 Chemical structure of the ligand **L** and synthesis of the metal complexes **1-4**.

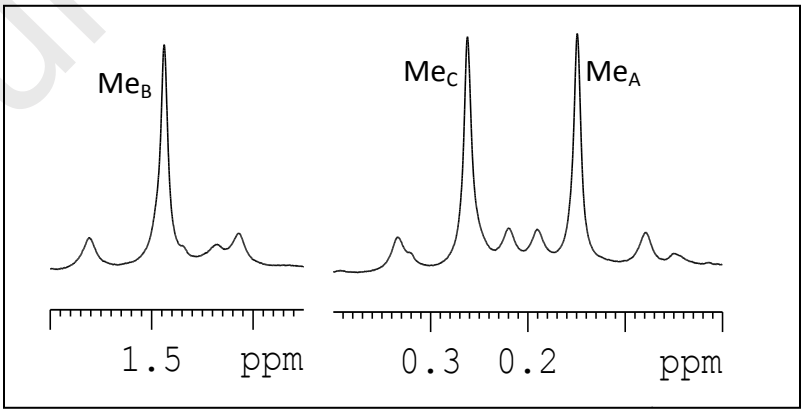

Figure 1 The satellite signals (due to ^{195}Pt-H coupling) for the methyl groups in the ^{1}H NMR spectrum of **4** in CD_2Cl_2 at -60 °C. For the labelling of the methyl protons, see Scheme 1.

X-ray crystallographic studies

Crystal structure of L

Yellow-orange needles of **L** suitable for X-ray diffraction analysis were obtained by the slow-diffusion of *n*-hexane vapors into its chloroform solution at room temperature. The ligand **L** crystallizes in the triclinic space group *P*-1 and the asymmetric unit consists of two crystallographically independent molecules. In both molecules, the terminal pyridine rings are oriented along the interannular bond in a *transoid* arrangement (Figure 2), a conformation typically observed in solid-state structures for terpyridines [33-36]. The interannular C−C bond lengths [1.487(2)-1.491(2) Å], C−C [1.3342(18)-1.3503(18) Å] and C−N bond lengths [1.375(2)-1.395(2) Å] in the pyridyl unit and the C−C bond lengths [1.378(2)-1.400(2) Å] in the phenyl rings are comparable with those in previously reported amino-terpyridines [33-36]. The two rings in the terpyridine part of **L** deviate only slightly from planarity as the twist angles between the pyridine N1, C1-C5/N5, C28-C32 rings and the central pyridine ring are 2.7 and 2.3°, while for the second pyridine N3, C11-C15/N7, C38-C42 rings the same angle is 25.2 and 24.5°, making the terpyridine part non-planar. The crystal packing shows $\pi\cdots\pi$ interactions (3.36 and 3.23 Å) between the terminal pyridine rings of neighboring molecules. In addition, weak N–H$\cdots\pi$ interactions between the aniline moiety and terminal pyridine nitrogen (marked as N3) could be observed in the 3-D crystal lattice.

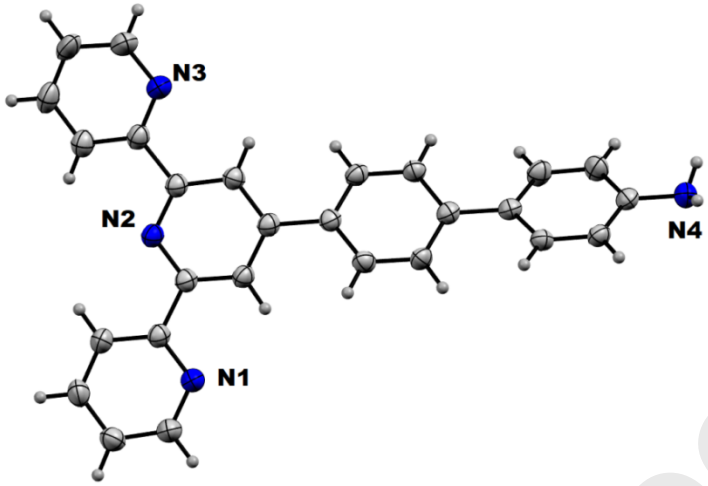

Figure 2 Crystal structure of ligand **L**. Thermal ellipsoids are shown at the 50% probability level. Nitrogen atoms are marked in a blue colour. Only one of the two crystallographically independent molecules is shown.

Crystal structures of 2-3

Single crystals of **2** and **3** were obtained by the slow diffusion of di-isopropyl ether into the corresponding acetonitrile solutions at room temperature. Complexes **2** and **3** are iso-structural, crystallizing in the monoclinic space group $P2_1/c$. The metal ions in the crystal structures of **2** and **3** show a distorted octahedral geometry, bound by six pyridyl nitrogen atoms (Figure 3). Selected bond lengths and angles are given in Table 1. The distortion in the geometry of the metal center arises due to the restricted bite angle of the terpyridine core, which results in shorter M–N bond distances [M = Zn, 2.053(6)-2.082(7) Å and M = Cd, 2.295(5)-2.301(5) Å] for the central pyridine ring than the terminal M–N distances of the pyridine rings [M = Zn, 2.164(7)-2.191(6) Å and M = Cd, 2.338(5)-3.364(5) Å]. These bond distances are similar to previously reported Zn^{II}/Cd^{II}-terpyridine complexes [23,37-39]. Unlike in the free ligand **L**, the terpyridine domains are approximately coplanar in **2** and **3**. The torsional angles between the terminal and central pyridine rings are in the range 3.5(4)-6.3(4)° for **2** and 3.1(3)-5.8(4)°) for **3**.

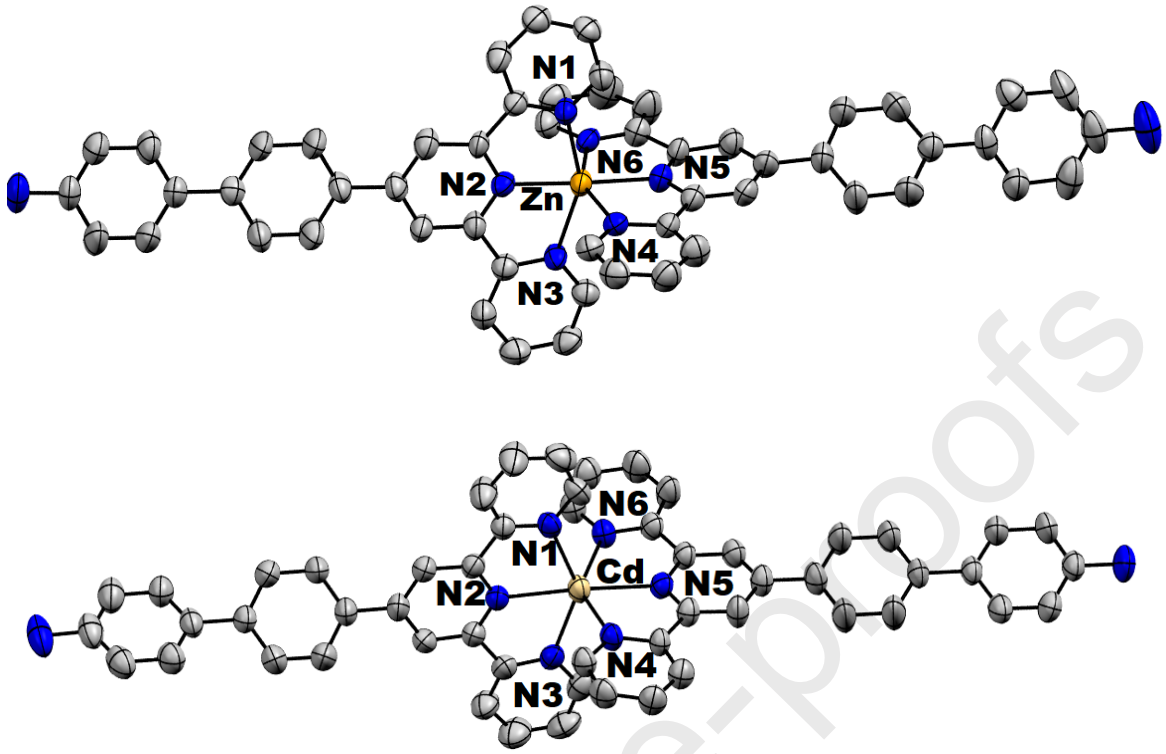

Figure 3 Crystal structures of complexes **2** (top), and **3** (bottom). Anions and hydrogen atoms are omitted for viewing clarity.

Crystal structure of 4

The yellow coloured single crystals of **4.(C_6H_6)** were obtained from an equimolar mixture of trimethylplatinum(IV) iodide and **L** in benzene upon standing. Complex **4** crystallizes in the monoclinic space group $P2_1/n$. The Pt(IV) center has a distorted octahedral geometry with three methyl groups in a *fac*-arrangement, together with two nitrogen atoms from **L** and an iodine ligand (Figure 4). Similar non-classical coordination modes of oligopyridine ligands have also been observed previously [23,31,32,40]. Selected bond lengths and angles are shown in Table 1. The Pt−N bond distance to the terminal pyridyl ring [2.149(13) Å] is shorter than the Pt-N bond distance to the central pyridyl ring [2.239(12) Å]. The Pt-I bond distance [2.8041(13) Å] and N-Pt-N bite angle [75.9(5) °] are comparable with those in previously reported Pt(IV)-terpyridine complexes [23,31,32]. The torsional angle between the central and the non-coordinated pyridyl ring [58.2(9)°] is larger compared to the Pt(IV)-coordinated pyridyl rings [21.9(8)°]. In the 3-D crystal lattice, **4** forms a 1-D hydrogen bonded polymer by $_{(py)}N\cdots H–N_{(amine)}$ intermolecular

hydrogen bonding involving the non-coordinated pyridyl ring nitrogen atom (marked as N3) and the aniline moiety, as shown in Figure S11 in the supporting information.

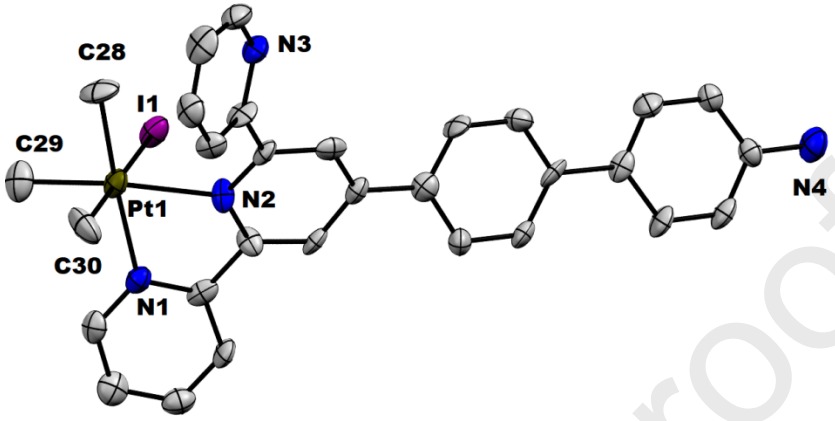

Figure 4 Crystal structure of **4**. The solvent molecule and hydrogen atoms are omitted for viewing clarity.

Table 1 Selected bond lengths (Å) and angles (°) for the ligand **L** and its metal complexes **2-4**

Ligand L[a]					
C1-N1	1.336(2)	C6-N2	1.347(2)	C11-N3	1.345(2)
C5-N1	1.342(2)	C10-N2	1.342(2)	C15-N3	1.342(2)
C1-C2	1.379(2)	C6-C7	1.384(2)	C11-C12	1.395(2)
C2-C3	1.377(2)	C7-C8	1.388(2)	C12-C13	1.380(2)
C3-C4	1.375(2)	C8-C9	1.397(2)	C13-C14	1.373(3)
C4-C5	1.386(2)	C9-C10	1.391(2)	C14-C15	1.383(3)
C5-C6	1.488(2)	C10-C11	1.489(2)	C25-N4	1.405(2)
C8-C16	1.486(2)	C19-C22	1.485(2)		
N1-C1-C2	123.82(16)	N1-C5-C4	121.96(15)	N1-C5-C6	116.52(14)
N2-C6-C5	116.88(14)	N2-C6-C7	122.72(14)	N2-C10-C11	115.65(14)
N2-C10-C9	123.15(14)	N3-C15-C14	123.50(19)	N3-C11-C12	122.26(15)
N3-C11-C10	117.46(15)	C1-N1-C5	117.78(15)	C6-N2-C10	117.29(14)
C11-N3-C15	117.61(16)	N4-C25-C26	120.07(14)	N4-C25-C24	121.66(15)
C8-C16-C21	120.08(14)	C19-C22-C23	122.42(14)	C19-C22-C27	121.40(14)
Complex 2		**Complex 3**		**Complex 4**	
Zn1-N1	2.191(6)	Cd1-N1	2.338(5)	Pt1-N1	2.149(13)
Zn1-N2	2.052(6)	Cd1-N2	2.295(5)	Pt1-N2	2.239(12)
Zn1-N3	2.183(6)	Cd1-N3	2.354(5)	Pt1-C28	2.048(16)
Zn1-N4	2.168(7)	Cd1-N4	2.347(5)	Pt1-C29	2.057(18)
Zn1-N5	2.086(7)	Cd1-N5	2.301(5)	Pt1-C30	2.06(2)
Zn1-N6	2.172(7)	Cd1-N6	2.364(5)	Pt1-I1	2.8041(13)

N1-Zn1-N2	75.3(2)	N1-Cd1-N2	70.40(17)	N1-Pt1-N2	75.9(5)
N1-Zn1-N3	150.8(2)	N1-Cd1-N3	139.92(17)	N1-Pt1-I1	88.8(4)
N1-Zn1-N4	95.4(2)	N1-Cd1-N4	105.39(18)	N1-Pt1-C28	176.5(7)
N1-Zn1-N5	102.1(2)	N1-Cd1-N5	116.80(18)	N1-Pt1-C29	96.7(7)
N1-Zn1-N6	91.8(2)	N1-Cd1-N6	90.57(17)	N1-Pt1-C30	88.6(6)
N2-Zn1-N3	75.7(2)	N2-Cd1-N3	69.84(17)	N2-Pt1-I1	86.7(3)
N2-Zn1-N4	105.2(3)	N2-Cd1-N4	110.01(17)	N2-Pt1-C28	100.6(7)
N2-Zn1-N5	177.4(2)	N2-Cd1-N5	172.63(19)	N2-Pt1-C29	171.5(6)
N2-Zn1-N6	103.9(3)	N2-Cd1-N6	109.07(18)	N2-Pt1-C30	94.6(7)
N3-Zn1-N4	89.2(2)	N3-Cd1-N4	92.61(18)	I1-Pt1-C28	91.7(6)
N3-Zn1-N5	106.9(2)	N3-Cd1-N5	102.85(17)	I1-Pt1-C29	88.9(5)
N3-Zn1-N6	98.0(2)	N3-Cd1-N6	97.67(18)	I1-Pt1-C30	176.6(5)
N4-Zn1-N5	75.2(3)	N4-Cd1-N5	70.46(17)	C28-Pt1-C29	86.8(8)
N4-Zn1-N6	150.9(2)	N4-Cd1-N6	140.78(17)	C28-Pt1-C30	91.1(8)
N5-Zn1-N6	75.7(3)	N5-Cd1-N6	70.36(18)	C29-Pt1-C30	89.3(8)
N7-C25-C24	120.0(9)	N7-C25-C24	121.3(7)	N4-C25-C24	120.3(15)
N7-C25-C26	121.8(9)	N7-C25-C26	120.0(7)	N4-C25-C26	122.8(15)
N8-C52-C51	119.5(12)	N8-C52-C51	120.5(9)	C10-C11-N3	115.7(15)
N8-C52-C53	122.6(12)	N8-C52-C53	120.3(9)	C10-C11-C12	119.6(15)

[a]Data is given for only one of the two crystallographically independent molecules in the unit cell.

Absorption spectroscopy

The ligand **L** shows an absorption maximum at 322 nm ($\varepsilon = 4.48 \times 10^4$ M^{-1} cm^{-1}) with a shoulder at 298 nm ($\varepsilon = 4.12 \times 10^4$ M^{-1} cm^{-1}) in dichloromethane (Figure 5). The lowest energy maximum corresponds to an Intramolecular Charge-Transfer (ICT) π_{ph}-π^*_{tpy} transition [9,18,41]. The absorption maximum for **L** is similar to the previously reported 4′-[4-(4-nitrophenyl)phenyl]-2,2′:6′,2′′-terpyridine [42] and is blue-shifted compared to 4′-(4-N,N-dimethylaminophenyl)phenyl-2,2′:6′,2′′-terpyridine [9] and 4′-[4-(4-N,N-dimethylaminophenyl)phenyl]-2,2′:6′,2′′-terpyridine [42]. The absorption maxima undergo a very small change when measured in solvents of higher polarity (Table 2 and Figure S10 in the supporting information).

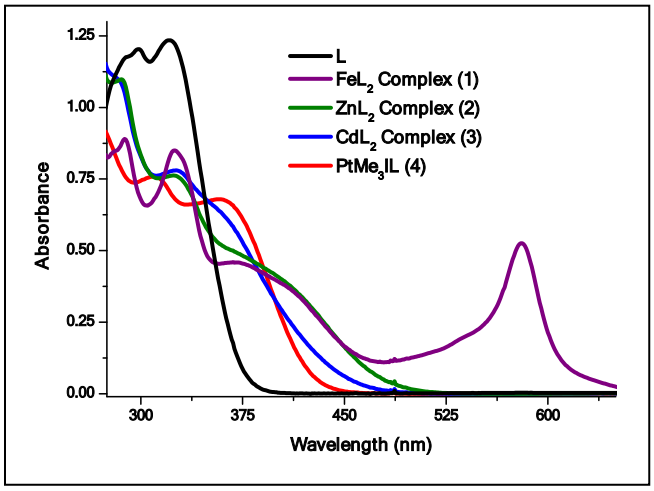

Figure 5 Room temperature UV-Vis absorption spectra of **L** and the metal complexes **1-4** in dichloromethane.

The absorption spectra of complexes **1-4**, measured in dichloromethane at room temperature, are also plotted in Figure 5. For all the complexes **1-4**, spin-allowed ligand-centered (LC) $\pi \rightarrow \pi^*$ transition(s) are observed between 315 and 325 nm. In addition, the peak at 360-385 nm corresponds to a metal induced intra-ligand charge transfer (ILCT) transition [43]. Moreover, complex **1** also shows a band at 580 nm which is due to a metal-to-ligand charge-transfer (MLCT) transition, observed in previously reported Fe(II)-terpyridine complexes [23,39]. Although the LC and MLCT transitions are not influenced by the solvent polarity, the ILCT transitions of the complexes **1-4** broadened in more polar solvents.

Emission spectroscopy

Upon UV-irradiation, **L** exhibits bright blue emission in dichloromethane and on excitation at 322 nm, a single intense band at 461 nm is observed in the emission spectrum. This indicates the fluorescence of **L** involves only one excited singlet state (Figure 6). The emission maximum of **L** shows a significant bathochromic shift with an increase in the solvent polarity (461 nm in dichloromethane to 533 nm in DMF) (Figure 6 and Table 2), indicating the presence of an ICT mechanism in the emissive excited-state of **L** [9,23]. In dichloromethane, a fluorescence quantum yield (Φ_F**)** as high as 0.68 is observed for **L** which is quite similar to the values for previously reported amino terpyridine compounds [18,41,44]. Further, measurement of Φ_F in different solvents shows that the fluorescence of **L** decreases with an increase in solvent polarity (Table 2). This result is further supported by the fact that the fluorescence lifetime of **L** also decreases on increasing the solvent polarity (Table 2), as is also observed for previously reported amino-terpyridine ligands [9,18,41]. In the solid-state, **L** does not show any fluorescence due to non-radiative deactivation pathways, possibly affected by intermolecular interactions. Similarly to our previous study [23], the fluorescence of **L**, being much weaker than the similar *p*-methoxy substituted ligand 4′-[4-{4-methoxyphenyl)ethynyl}phenyl]-2,2′:6′,2′′-terpyridine (Φ_F = 0.78 in dichloromethane), is markedly reduced upon complexation with Zn(II) and Cd(II) ions, while the other metal ions,

Fe(II) and Pt(IV), completely quench the fluorescence of **L**. The quenching of ligand fluorescence upon metal complexation is a common phenomenon, possibly affected by electron transfer or an energy transfer mechanism [45]. The weak fluorescence of the Zn(II) and Cd(II) complexes is due to an ILCT transition from the amine moiety to the metal coordinated terpyridine fragment [9,23,46]. The non-fluorescence nature of the Fe(II)-terpyridine complex is most likely because of a change of the MLCT type singlet excited state, ^{1}MLCT, to the corresponding short lived triplet state, ^{3}MLCT [47]. On the other hand, the fluxional behavior of the terpyridine ligand could play a significant role in the quenching of fluorescence in the Pt(IV) complex.

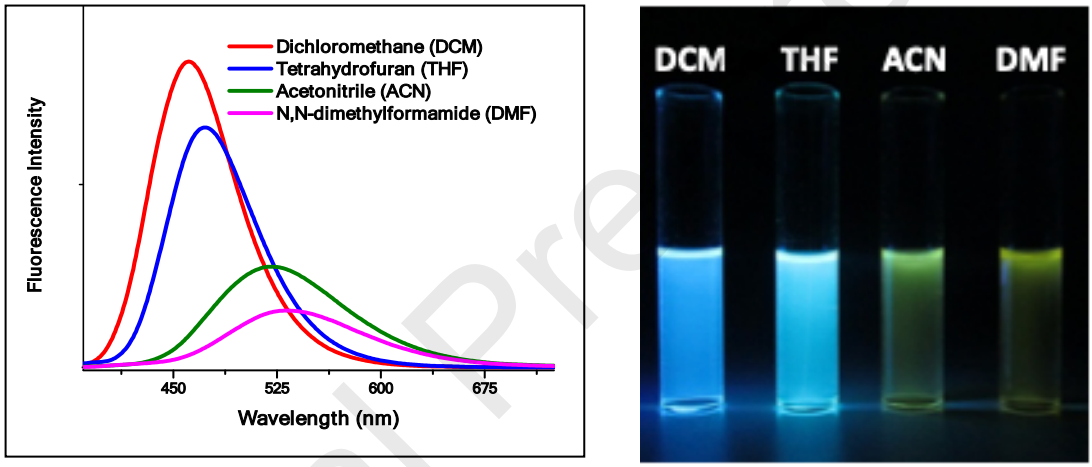

Figure 6 Fluorescence spectra (left) and colour (right) of **L** in different solvents at room temperature.

Table 2 Absorption and emission properties of **L** in different solvents

Solvent	λ_{max}^{abs} **(nm)**^{a}	λ_{max}^{em} **(nm)**^{b}	$\Phi_F{}^{c}$	τ_F **(ns)**^{d}
Dichloromethane	322	461	0.68	2.93
Tetrahydrofuran	326	474	0.63	2.24
Acetonitrile	328	520	0.10	1.22
N,N-Dimethylformamide	337	533	0.05	-

^{a}Lowest energy absorption band. ^{b}Upon excitation of the lowest energy absorption band. ^{c}Relative fluorescence quantum yield. ^{d}Fluorescence lifetime.

Conclusions

In conclusion, the synthesis and characterization of four new transition metal complexes of the amino terpyridine ligand 4′-[4-(4-aminophenyl)phenyl]-2,2′:6′,2′′-terpyridine **L**, $[Fe\mathbf{L}_2](ClO_4)_2$ (**1**), $[Zn\mathbf{L}_2](ClO_4)_2$ (**2**), $[Cd\mathbf{L}_2](ClO_4)_2$ (**3**) and $[PtMe_3I\mathbf{L}]$ (**4**), are discussed. Complexes **1-3** were synthesized by the reaction of metal ions with **L** in a 1:2 ratio, while the reaction of an equimolar mixture of **L** and $PtMe_3I$ resulted the formation of **4**. The complexes were characterized by ^1H NMR spectroscopy, Mass spectroscopy, CHN analysis and an X-ray single crystal study. The X-ray crystal structure analysis of complexes **2** and **3** shows the tridentate coordination of **L** to the metal centre, while the structural investigation of **4** confirms the bidentate coordination mode of **L**. The X-ray crystal structure of **L** shows a *trans*-arrangement of the terminal pyridine nitrogen atoms with respect to central pyridine ring in the terpyridine backbone. The photophysical studies show that **L** is highly fluorescent in non-polar solvents, with an emission maximum that shows a significant bathochromic shift upon increasing the solvent polarity. The fluorescence of **L** is reduced significantly upon complexation, with the Zn(II) and Cd(II) complexes showing only very weak fluorescence, while complexes **1** and **4** were found to be non-fluorescent.

Appendix A. Supplementary data

CCDC 1901884-1901887 contain the supplementary crystallographic data for **L** and complexes **2-4**. These data can be obtained free of charge via http://www.ccdc.cam.ac.uk/conts/retrieving.html, or from the Cambridge Crystallographic Data Centre, 12 Union Road, Cambridge CB2 1EZ, UK; fax: (+44) 1223-336-033; or e-mail: deposit@ccdc.cam.ac.uk.

Acknowledgments

We thank Dr. Elina Kalenius for measurement of the mass spectra. The authors gratefully acknowledge financial support from the Academy of Finland (RP: grant no. 298817) and the University of Jyväskylä.

Conflicts of interest

There are no conflicts to declare

References

[1] U. S. Schubert, H. Hofmeier, G. R. Newkome, Modern terpyridine chemistry, Wiley-VCH, Weinheim, 2006.

[2] A. Wild, A. Winter, F. Schlütter, U. S. Schubert, Chem. Soc. Rev. 40 (2011) 1459-1511.

[3] E. C. Constable, Chem. Soc. Rev. 36 (2007) 246-253.

[4] M. W. Cooke, G. S. Hanan, Chem. Soc. Rev. 36 (2007) 1466-1476.

[5] B.-B. Cui, J.-Y. Shao, Y.-W. Zhong, Organometallics 33 (2014) 4220−4229.

[6] H.-J. Nie, C.-J. Yao, M.-J. Sun, Y.-W. Zhong, J. Yao, Organometallics 33 (2014) 6223-6231.

[7] K.-Q. Wu, J. Guo, J.-F. Yan, L.-L. Xie, F.-B. Xu, S. Bai, P. Nockemann, Y.-F. Yuan, Organometallics 30 (2011) 3504-3511.

[8] C.-J. Yao, J. Yao, Y.-W. Zhong, Inorg. Chem. 50 (2011) 6847–6849.

[9] W. Goodall, J. A. G. Williams, Chem. Commun. (2001) 2514–2515.

[10] B. N. Ghosh, S. Bhowmik, P. Mal, K. Rissanen, Chem. Commun. 50 (2014) 734-736.

[11] S. Bhowmik, B. N. Ghosh, K. Rissanen, Org. Biomol. Chem. 12 (2014) 8836-8839.

[12] G. Hughes, M. R. Bryce, J. Mater. Chem. 15 (2005) 94–107.

[13] Y.-M. Zhang, S.-H. Wu, C.-J. Yao, H.-J. Nie, Y.-W. Zhong, Inorg. Chem. 51 (2012) 11387-11395.

[14] W. Kaim, G. K. Lahiri, Angew. Chem. Int. Ed. 46 (2007) 1778-1796.

[15] S. Bhowmik, B. N. Ghosh, V. Marjomäki, K. Rissanen, J. Am. Chem. Soc. 136 (2014) 5543-5546.

[16] L. J. Liang, X. J. Zhao, C. Z. Huang, Analyst 137 (2012) 953-958.

[17] P. Das, A. Ghosh, M. K. Kesharwani, V. Ramu, B. Ganguly, A. Das, Eur. J. Inorg. Chem. (2011) 3050-3058.

[18] J.-D. Cheon, T. Mutai, K. Araki, Org. Biomol. Chem. 5 (2007) 2762-2766.

[19] J. C. Loren, J. S. Siegel, Angew. Chem. Int. Ed. 40 (2001) 754-757.

[20] A. Maroń, A. Szlapa, T. Klemens, S. Kula, B. Machura, S. Krompiec, J. G. Matecki, A. Świtlicka-Olszewska, K. Erfurt, A. Chrobok, Org. Biomol. Chem. 14 (2016) 3793-3808.

[21] A. Winter, C. Friebe, M. D. Hager, U. S. Schubert, Eur. J. Org. Chem. (2009) 801-809.

[22] A. Winter, D. A. M. Egbe, U. S. Schubert, Org. Lett. 9 (2007) 2345-2348.

[23] B. N. Ghosh, F. Topić, P. K. Sahoo, P. Mal, J. Linnera, E. Kalenius, H. M. Tuononen, K. Rissanen, Dalton Trans. 44 (2015) 254-267.

[24] Rigaku Oxford Diffraction, CrysAlisPro software system, version 38.46, Rigaku Corporation, Oxford, UK 2017.

[25] Bruker AXS BV, Madison, WI, USA 1997–2004.

[26] R. W. Hooft, in COLLECT, Nonius BV, Delft, The Netherlands 1998.

[27] Z. Otwinowski, W. Minor, Methods Enzymol. 276 (1997) 307–326.

[28] G. M. Sheldrick, SADABS, Bruker Analytical X-ray system, Inc., Madison, Wisconsin 2008.

[29] (a) G. M. Sheldrick, Acta Cryst. A64 (2008)112–122; (b) G.M. Sheldrick, Acta Cryst. C71 (2015) 3–8.

[30] O. V. Dolomanov, L. J. Bourhis, R. J. Gildea, J. A. K. Howard, H. J. Puschmann, J. Appl. Cryst. 42 (2009) 339–341.

[31] B. N. Ghosh, M. Lahtinen, E. Kalenius, P. Mal, K. Rissanen, Cryst. Growth Des. 16 (2016) 2527-2534.

[32] E. W. Abel, V. S. Dimitrov, N. J. Long, K. G. Orrell, A. G. Osborne, V. Šik, M. B. Hursthouse, M. A. Mazid, J. Chem. Soc., Dalton Trans. (1993) 291-298.

[33] B. Liu, Q. Zhang, H. Ding, G. Hu, Y. Du, C. Wang, J. Wu, S. Li, H. Zhou, J. Yang, Y. Tian, Dyes Pigm. 95 (2012) 149-160.

[34] F. Emmerling, J. L. Bricks, U. Resch-Genger, W. Kraus, B. Schulz, Y. Q. Li, G. Reck, J. Mol. Struct. 874 (2008) 14-27.

[35] R.-A. Fallahpour, M. Neuburge, M. Zehnder, New J. Chem. 23 (1999) 53-61.

[36] G. D. Storrier, S. B. Colbran, D. C. Craig, J. Chem. Soc., Dalton Trans. (1997) 3011-3028.

[37] Y. H. Lee, E. Kubota, A. Fuyuhiro, S. Kawata, J. M. Harrowfield, Y. Kim, S. Hayami, Dalton Trans. 41 (2012) 10825-10831.

[38] E. C. Constable, C. E. Housecroft, N. S. Murray, J. A. Zampese, Polyhedron 54 (2013) 110-118.

[39] N. W. Alcock, P. R. Barker, J. M. Haider, M. J. Hannon, C. L. Painting, Z. Pikramenou, E. A. Plummer, K. Rissanen, P. Saarenketo, J. Chem. Soc., Dalton Trans. (2000) 1447-1462.

[40] E. C. Constable, C. E. Housecroft, Coord. Chem. Rev. 350 (2017) 84-104.

[41] T. Mutai, J.-D. Cheon, G. Tsuchiya, K. Araki, J. Chem. Soc., Perkin Trans. 2 (2002) 862-865.

[42] W. Goodall, K. Wild, K. J. Arm, J. A. G. Williams, J. Chem. Soc., Perkin Trans. 2 (2002) 1669-1681.

[43] X. Chen, Q. Zhou, Y. Cheng, Y. Geng, D. Ma, Z. Xie, L. Wang, J. Luminescence 126 (2007) 81-90.

[44] T. Klemens, A. Świtlicka, B. Machura, S. Kula, S. Krompiec, K. Laba, M. Korzec, M. Siwy, H. Janeczek, E. Schab-Balcerzak, M. Szalkowski, J. Grzelak, S. Maćkowski, Dyes Pigm. 163 (2019) 86-101.

[45] J. A. Kemlo, T. M. Sheperd, Chem. Phys. Lett. 47 (1977) 158-162.

[46] E. A. Medlycott, G. S. Hanan, Chem. Soc. Rev. 34 (2005) 133-142.

[47] X.-y. Wang, A. D. Guerzo, R. H. Schmehl, Chem. Commun. (2002) 2344-2345.

Author's Contribution Section:

Biswa Nath Ghosh: Methodology, Absorption and Emission study, writing original draft preparation

Rakesh Puttreddy: Data collection, solving crystal structures

Kari Rissanen: Conceptualization, Writing reviewing, editing.

Graphical Abstract_Pictogram

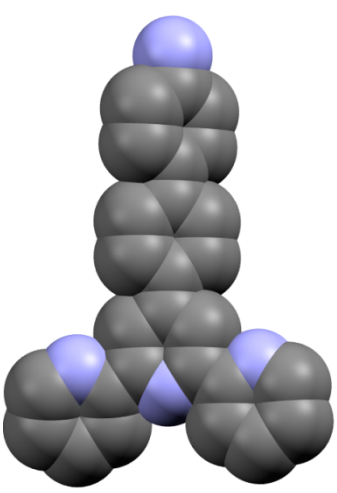

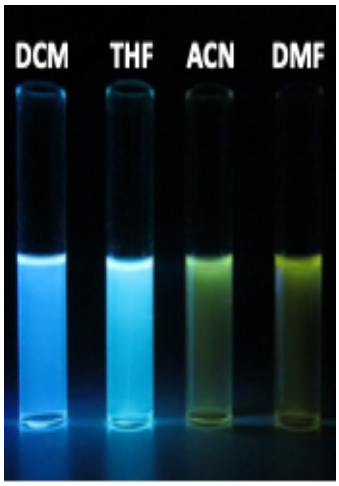

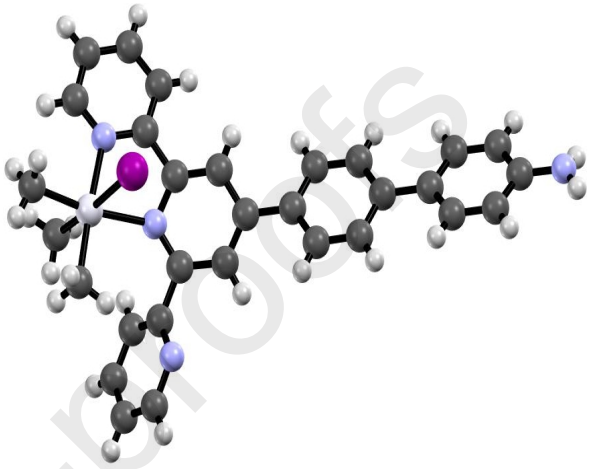

Graphical Abstract Synopsis

The synthesis and structural characterization of four new metal complexes of the highly luminescent amino-terpyridine ligand 4′-[4-(4-aminophenyl)phenyl]-2,2′:6′,2″-terpyridine **L**, [Fe**L**$_2$](ClO$_4$)$_2$ (**1**), [Zn**L**$_2$](ClO$_4$)$_2$ (**2**), [Cd**L**$_2$](ClO$_4$)$_2$ (**3**) and [PtMe$_3$I**L**] (**4**), are reported. Structural analysis confirms that **L** forms a bidentate complex with the platinum(IV) ion, while tridentate complexes are formed with the divalent metal ions (Fe^{2+}, Zn^{2+} and Cd^{2+}). Further, the crystal structure of **L** shows a *transoid* conformation of the pyridine ring nitrogen atoms along the interannular bond in the terpyridine domain. A photophysical study shows that **L** is *highly fluorescent in solution* (Φ_F = 0.68 in dichloromethane) with an emission maximum that shows significant solvatochromism.